Supporting Information

New HOPE-enabled photoacoustic imaging of water: enhanced contrast, dynamic range, and multifaceted applications

Huajun Tang, Yitian Tong, Mingsheng Li, Najia Sharmin, Jiawei Shi, Bingfeng Li, Chandra Jinata, Nikki Pui-Yue Lee, Kevin K. Tsia and Kenneth K. Y. Wong**

1. PM coil in the experiment setup

In the proposed scheme, a long optical fiber is used as a feedback path to reduce the repetition rate of the output pulses. Long optical fiber links are susceptible to temperature and environmental mechanical jitter, which causes phase jitter of the transmitted optical signal. That will affect the time jitter of the output pulse. In order to minimize the effect, a compact PM coil (YOFC, CQ1-I52/12-PM) with 1.04 km long is adopted as shown in Fig. S1, which is used multi-pole symmetrical winding method. High mechanical stability and low temperature drift characteristics of the PM coil greatly improve the stability of the oscillation loop. At the same time, its high polarization extinction ratio ensures polarization stability.

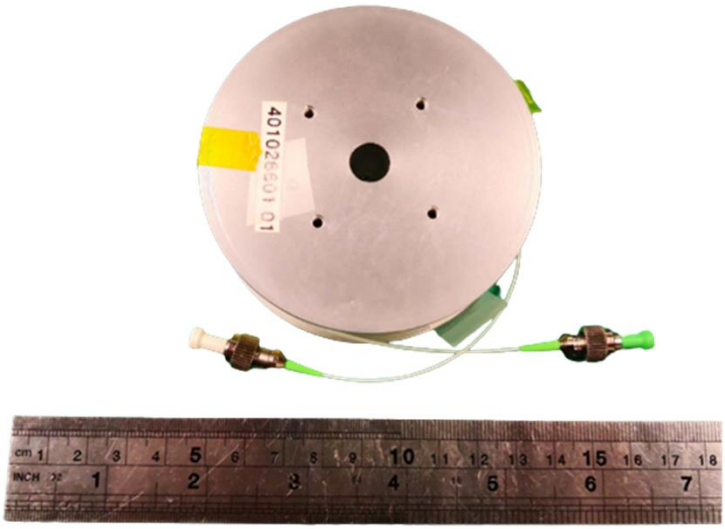

Fig. S1. The diagram of the PM coil.

2. Flexible pulse width of new HOPE

Through the precise adjustment of the fiber delay line, the modulation frequency coincides with the resonant frequency of the cavity. Thus, the generated pulse can maintain stable oscillation within a certain range. Just by tuning the function generator's delivering pulse width to the EML, the new HOPE's pulse width can be continuously tuned from 4 ns to 15 ns without any hardware replacement. Some integer pulse width results are shown in Fig. S2. From the results, the width of the generated pulse in the tuning range is changed, while the pulse shape remains basically the same. As the pulse width increases, the pulse peak power decreases, which is due to the fixed average power.

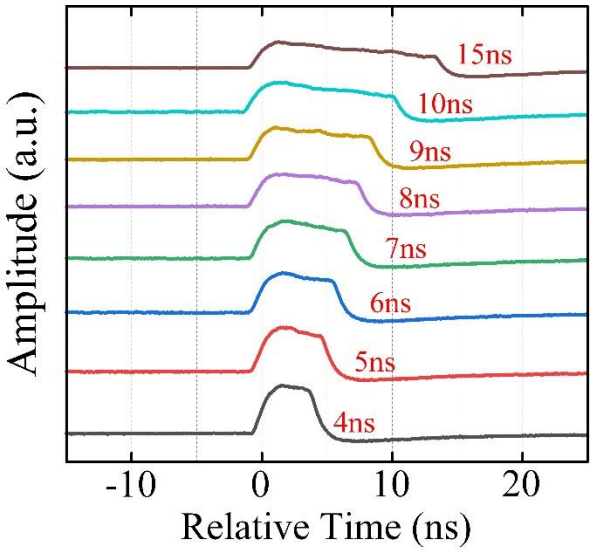

Fig. S2. Different pulse width generated by the new HOPE via tuning the delivering pulse width of the function generator.

3. Image subtraction procedure for adipose tissue image enhancement

The image subtraction procedure takes two images as input and produces the result whose pixel values are those of the PA image of 1750 nm minus the corresponding pixel values from the PA image of 1930 nm. Considering the different signal intensity ratios of the water and lipid at two different wavelengths, the images need to be normalized and multiplied by the corresponding coefficients for the two images before image subtraction, respectively. The output pixel values are given by:

$$Q_{lipid}(i,j) = P_{normalized-lipid}(i,j) \times C_{lipid} - P_{normalized-water}(i,j) \times C_{water} \quad \text{(S1)}$$

where the $P_{normalized-lipid}$ and $P_{normalized-water}$ are the normalized intensity of the pixels in images of the lipid and water, respectively. The C_{lipid} and C_{water} are the coefficients of lipid-to-water at 1750 nm and water-to-lipid at 1930 nm, which can be given by:

$$C_{lipid} = I_{lipid-1750\,nm}/I_{water-1750\,nm}$$

$$C_{water} = I_{water-1930\,nm}/I_{lipid-1930\,nm} \quad \text{(S2)}$$

where the $I_{lipid-1750\,nm}$ is the PA signal intensity of butter at 1750 nm, the $I_{water-1750\,nm}$ is the PA signal intensity of water at 1750 nm, while the $I_{water-1930\,nm}$ represents the PA signal intensity of water at 1930 nm, and the $I_{lipid-1930\,nm}$ represents the PA signal intensity of butter at 1930 nm. The C_{water} is calculated to be ~36 according to the results shown in the Fig. 5a and b. Meanwhile, the C_{lipid} is calculated to be ~14 according to the results shown in the Fig. S3. Above results roughly match the report in Ref. 44.

The results of the image subtraction are finally processed in ImageJ for adjusting the contrast/balance, and finally coloring.

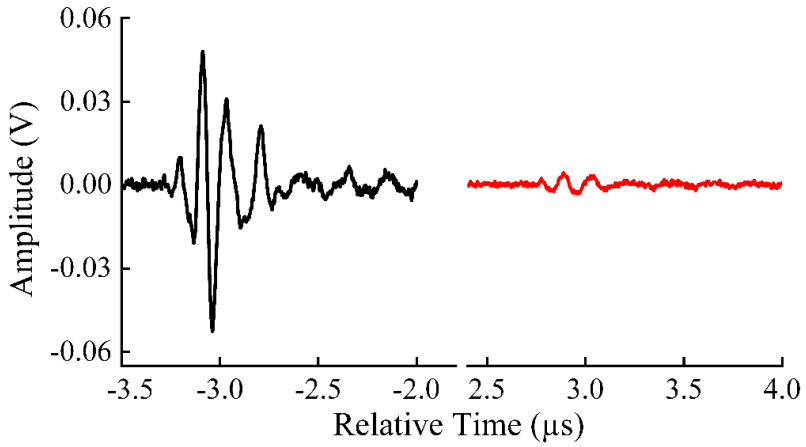

Fig. S3. PA signal of butter (black) and water (red) obtained at 1750 nm.

4. Spatial resolutions of the imaging system

To characterize the PA microscope imaging system, we measure the lateral resolution, axial resolution, and depth of field (DOF) of the imaging system, respectively. The lateral resolution of the system is measured by scanning a sharp edge submerged in silicon oil, parallel to the Y-axis. The sample is scanned across by 2 μm steps. The PA signal values are fitted by a sigmoidal-shaped function to get the fitted edge spread function (ESF) of the system, as shown in Fig. S4a. Then, the full width at half maximum (FWHM) of the line spread function (LSF) is calculated to be around 19 μm as shown in Fig. S4b, which is the derivative concerning ESF.

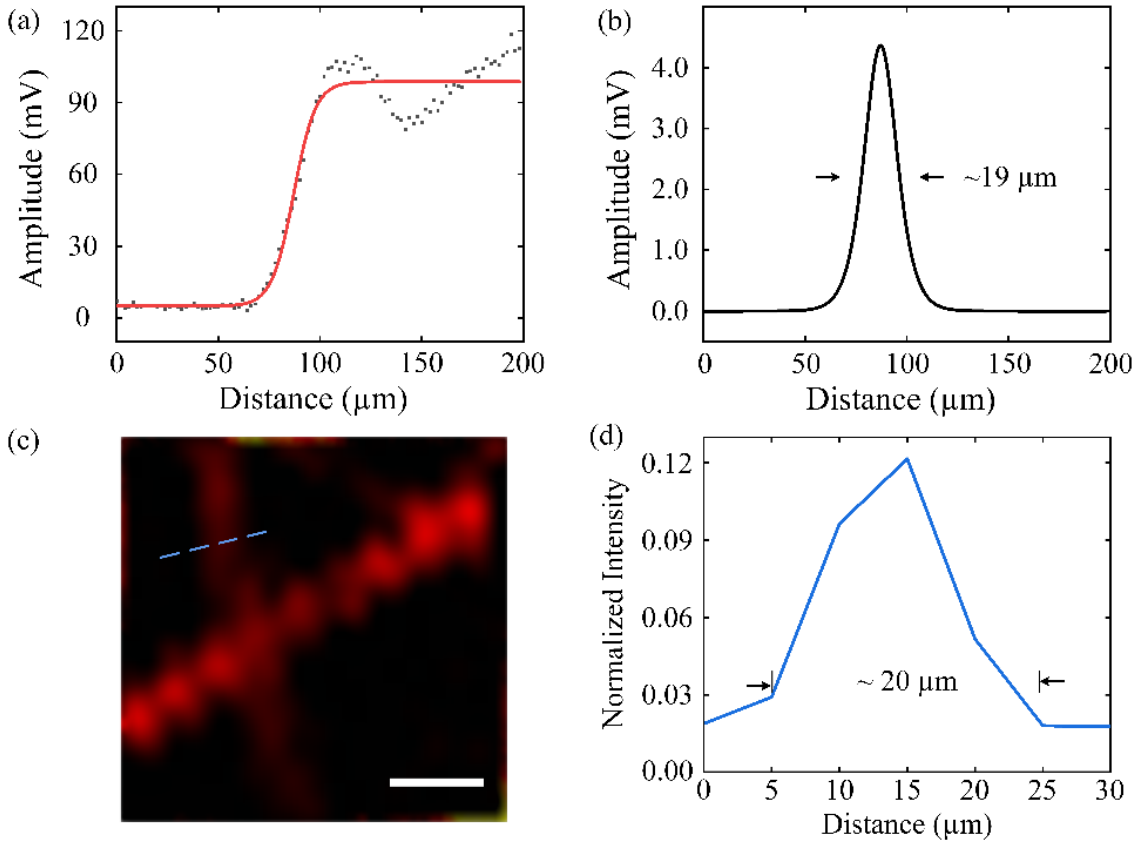

Fig. S4. Lateral resolution characterization by imaging a sharp edge and carbon fibers. a) The photoacoustic signal of the sharp edge (black dot) in one line of Y-axis, and its theoretical fit (red line). b) The LSF of the imaging system calculated by the ESF according to the results in Fig. a. c) The PA image of carbon fibers (scale bar: 25 μm). d) The intensity profile plot of the blue dashed line in Fig. c.

To testify to the lateral resolution of the system, the carbon fibers submerged in silicon oil are also imaged by 5 μm steps, as shown in Fig. S4c. The width of the carbon fiber is measured to be around

20 μm based on a cross-sectional profile of the carbon fiber in the blue dashed line shown in Fig. S4d. That can still characterize the lateral resolution of the imaging system. These two results match each other roughly and indicate that the system has a lateral resolution of around 20 μm. Theoretically, the ideal lateral resolution of the system is about 4 μm. The reason for this difference is mainly due to the mismatch of the used objective lens with the corresponding waveband, which results in parameter deterioration.

The axial resolution is determined by taking the FWHM of the PA signal envelope in the depth direction. The Hilbert transform is applied to the PA signal for water in Fig. 4a to obtain the envelope, as shown in Fig. S5. The FWHM of the envelope is calculated to be around 203.1 μm corresponding to axial resolution of the system. According to the calculation, the theoretical axial resolution of the system is 188.6 μm. The actual system is basically consistent with the theoretical value.

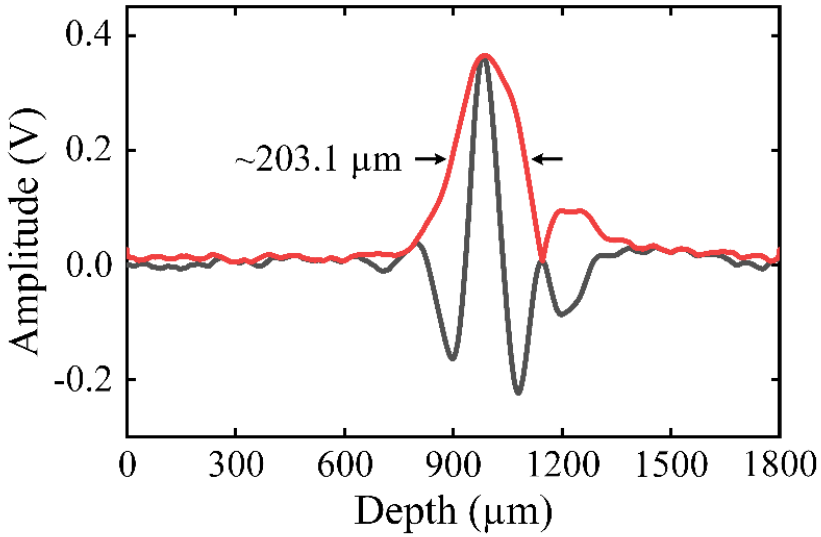

Fig. S5. Axial resolution characterization by the envelope of the water signal.

Further, the distance between the objective lens and the sample (water) is varied at 0.25 mm steps to determine the DOF of the system. The variation of intensity of the PA signal with the distance from the objective to the sample is recorded and then fitted by Gaussian fitting, as shown in **Fig. S6**. From the results, the DOF is calculated to be around 1.95 mm.

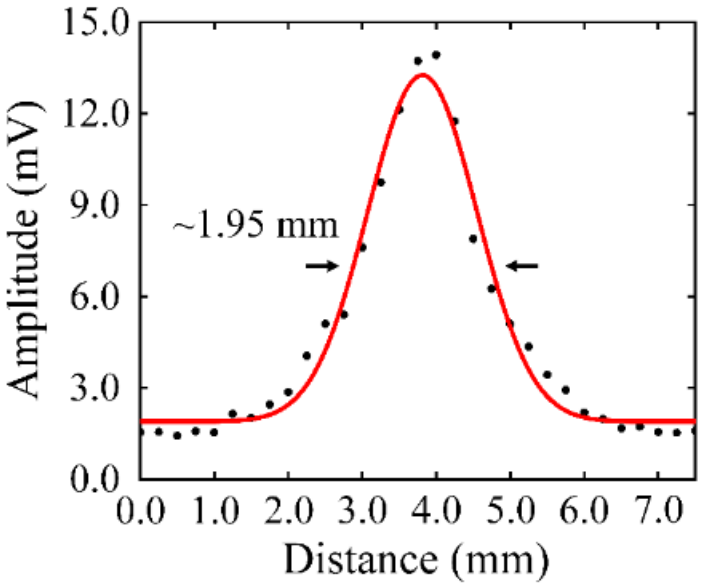

Fig. S6. Characterization of the DOF of the system.

Note that, scattering changes the propagation path of PA pump photons. Within one transport mean free path, the quasi-ballistic photons experience several scattering events but most of them keep the propagation direction [57]. Thus, the spatial resolution is not significantly deteriorated. Here, one transport mean free path of 1930-nm photons in soft tissue is ~2.5 mm [58, 59], thus, the spatial resolution is still determined by the diffractive limit of the pump beam. With a deeper penetration depth over one transport mean free path, the resolution is expected to deteriorate.

5. Pulse-to-pulse time jitter

Pulse-to-pulse time jitter represents the extent to which the waveform over the zero point deviates from its temporally ideal position in time domain, that is, is corrupted. Another definition is that each cycle deviates from its ideal value. These definitions differ slightly, resulting in several calculations of jitter. To describe time jitter quantitatively, the deviation of each positive (or negative) edge point of the time-domain pulse from an ideal reference signal can be measured, i.e. ΔT_1, ΔT_2, etc. This is called absolute time jitter because it is derived from a comparison with an ideal reference signal. The root mean square of the absolute time jitter is calculated as:

$$\Delta T_{abs,rms} = \lim_{N\to\infty} \frac{1}{N} \sqrt{\Delta T_1^2 + \Delta T_2^2 + \Delta T_3^2 + \cdots + \Delta T_N^2} \quad \text{(S3)}$$

Another type of time jitter is period time jitter, which is defined as the deviation of each cycle of the waveform from the mean value $\bar{T}$, shown as:

$$\Delta T_{p,rms} = \lim_{N\to\infty} \frac{1}{N} \sqrt{(\bar{T} - T_1)^2 + (\bar{T} - T_2)^2 + \cdots + (\bar{T} - T_N)^2} \quad \text{(S4)}$$

Both absolute and periodic time jitter can be used to describe signal quality in the time domain. In the manuscript, the pulse-to-pulse time jitter is periodic time jitter, calculated by Eq. S4.

We take 1000 continuous pulses for calculation. After an interval of 1 hour, we take the same 1000 pulses for calculation, and compare the time jitter changes.